Synthesis and Crystallization of N-rich Triazole Compounds

crystals

MDPI

Article

Synthesis and Crystallization of N-Rich Triazole Compounds

Emmanuele Parisi [1,*] and Roberto Centore [2]

[1] Department of Science and Applied Technology, Politecnico di Torino, Corso Duca degli Abruzzi 24, I-10129 Torino, Italy
[2] Department of Chemical Sciences, Università degli Studi di Napoli Federico II, Via Cinthia, I-80126 Napoli, Italy; roberto.centore@unina.it
* Correspondence: emmanuele.parisi@polito.it

Abstract: Among N-rich heterocycle backbone compounds, the triazoles building block received a lot of interest in several different academic and industrial studies and applications. This article outlines the process of synthesizing three different 1,2,4-triazole-based systems, commencing with 1,3-diaminoguanidine hydrochloride monohydrate as the starting material. The five novel crystal structures, **Triaz1**, **Triaz2**, **Triaz3**, **Triaz4**, **and Triaz5**, were characterized by NMR spectroscopy and single-crystal X-ray diffraction analysis. Hirshfeld surface analysis was employed to explore the intermolecular interactions that are responsible for quantitative crystal packing. The synthesized compounds, with their elevated nitrogen content, serve as potential components for High-Energy-Density material science applications.

Keywords: crystal engineering; N-rich compounds; triazole system; HEDM; Hirshfeld surface

Citation: Parisi, E.; Centore, R. Synthesis and Crystallization of N-Rich Triazole Compounds. *Crystals* **2023**, *13*, 1651. https://doi.org/10.3390/cryst13121651

Academic Editor: Shigeyuki Yamada

Received: 30 October 2023
Revised: 28 November 2023
Accepted: 28 November 2023
Published: 30 November 2023

1. Introduction

Heterocyclic compounds and nitrogen-rich hetero compounds are widespread in nature and play numerous roles in the physiology of living organisms. They are present in vitamins, in amino acids (proline, histidine and tryptophan), in biologically active compounds [1], such as chlorophyll and heme (structurally consisting of derivatives of porphyrins rings), in medicines (including anti-inflammatory, antimalarial, antimicrobial, antiviral and antidiabetic ones), in synthetic agrochemicals (herbicides and insecticides) and in natural bioactive substances, such as alkaloids, caffeine, etc. Undoubtedly, it is crucial to highlight their significance as fundamental biological molecules that constitute DNA and RNA. Moreover, the growing utilization of N-rich aromatics as foundational components for crafting conjugated active molecules with applications across a range of advanced materials fields, including semiconducting polymers [2,3], organic field-effect transistors [4,5], fluorescent sensors [6,7], organic solar cells [8,9] and high-energy-density compounds [10–13], merits attention. An intriguing and peculiar feature of many heterocyclic systems with a high nitrogen content is tautomerism [14–18]. Tautomerization reactions typically entail the shifting of a lone hydrogen atom, which is why they are commonly linked to molecules that have acidic functional groups. This holds particular relevance in the context of crystal engineering because the precise location of a hydrogen atom within the molecule significantly influences its potential to establish hydrogen bonds. Consequently, this has implications for synthon formation and, consequently, the overall packing arrangement. Quasi-degenerate tautomers are a fascinating occurrence. In this case, in fact, the equilibrium mixture contains appreciable amounts of all tautomers. Crystallization represents one of the limited methods available for the separation of distinct tautomers, primarily because it is unlikely to detect various tautomeric forms within the same crystal structure [19]. For quasi-degenerate tautomeric systems, the co-crystallization of two tautomers in the same lattice is a possibility but still a rare phenomenon; another possibility is the precipitation of different crystal forms, each with its own tautomer. These

two occurrences account for no more than 0.5% of molecules in the Cambridge Structural Database, which is another reason why quasi-degenerate tautomeric systems are particularly interesting. In recent years, our focus has been directed toward the synthesis and examination of benzimidazole [20–22] and N-rich triazole derivatives [7,12,16,17,23] in order to investigate their chemico-physical properties and tautomerism. Here, we report the synthesis and crystallization of five novel N-rich triazole systems with a nitrogen content between 55 and 70% *w*/*w*, which are potentially of interest for HEDMs applications (Scheme 1). In this context, energetic heterocyclic compounds with a high nitrogen content have emerged as a viable alternative to traditional HEDMs because of their higher stability and environmental friendliness [24]. Energetic materials typically release energy through oxidation processes when they decompose, and nitrogen-rich heterocyclic compounds are no exception. These compounds contain nitrogen atoms that are often involved in single or double bonds, and when the molecule decomposes, it generates N_2. The production of nitrogen gas as the primary byproduct makes the entire process environmentally friendly. This effect becomes more pronounced as the nitrogen content of the molecule increases, as it leads to reduced quantities of other byproducts. Furthermore, an increased nitrogen-to-carbon and hydrogen ratio enhances density, which is also desirable. Another valuable aspect of nitrogen-rich heterocyclic compounds is the presence of acidic or basic functional groups, often in the form of basic nitrogen atoms or acidic N-H groups. These features can be harnessed to form salts, where the nitrogen-rich heterocycle serves as a cation or anion. Such salts typically exhibit a high stability and can possess diverse properties, depending on the choice of counterion.

Triaz1

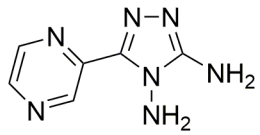

5-(pyrazin-2-yl)-4*H*-1,2,4-triazole-3,4-diamine

Triaz2

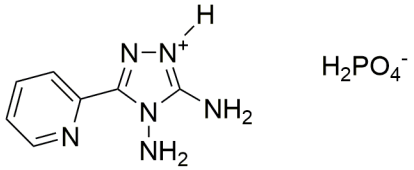

4,5-diamino-3-(pyridin-2-yl)-4*H*-1,2,4-triazol-1-ium dihydrogenphosphate

Triaz3

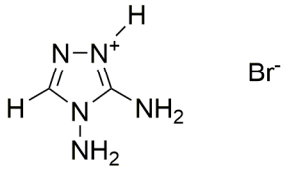

4,5-diamino-4*H*-1,2,4-triazol-1-ium bromide

Triaz4

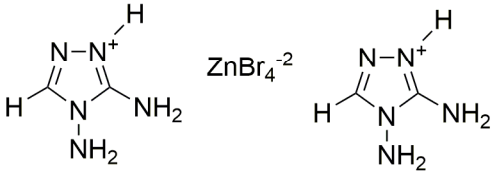

bis(4,5-diamino-4*H*-1,2,4-triazol-1-ium) zinc(II) tetrabromide

Triaz5

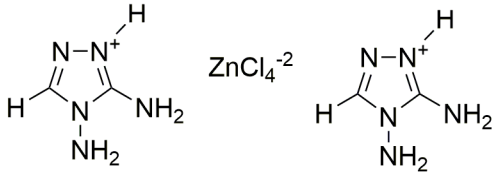

bis(4,5-diamino-4*H*-1,2,4-triazol-1-ium) zinc(II) tetrachloride

Scheme 1. The five novel diaminotriazole compounds described in this paper.

2. Experimental Section

2.1. Materials and Methods

Caution! The title complexes possess the potential to function as high-energy materials that may detonate under specific circumstances. Despite our incident-free experience in the preparation and handling of these complexes, it is crucial to recognize their energetic nature. Therefore, it is advisable to implement proper safety precautions, including wearing protective gear, such as leather coats, safety glasses, face shields, and ear plugs, particularly when working with these compounds on a larger scale.

Starting materials were purchased from Sigma Aldrich (Italy), AlfaAesar (Italy) and Fluorochem (UK) and used without further purification. All solvents were used with analytical grade. **3,4-diamino-1,24-triazolium chloride (DATr-HCl)** was synthesized according to a literature procedure [25]. **Triaz1** and **Triaz2** were synthetized by following a slightly modified version of a literature procedure [26]. The synthetic procedures are reported in detail below.

2.1.1. NMR Spectroscopy

The compounds' identity was confirmed by Bruker Avance 400 MHz, Varian Inova 500 MHz NMR spectrometers (Netherlands). ^{1}H-NMR and ^{13}C-NMR spectra were recorded by using d_6-DMSO solvent.

2.1.2. Melting Point Determination

The melting points of compounds were determined by temperature ramp measurements with a Mettler FP90 heating stage (Netherlands), heating rate of 10 °C/min, equipped with a polarizing Zeiss Axioskop (Germany).

2.1.3. X-ray Single Crystal Analysis

All data for crystal structure determinations were measured on a Bruker-Nonius KappaCCD diffractometer (Netherlands) equipped with an Oxford Cryostream 700 apparatus, using graphite monochromated MoKα radiation (0.71073 Å). Data were collected at room temperature and at −100 °C. Reduction of data and semiempirical absorption correction were done using SADABS program [27]. The structures were solved by direct methods (SIR97 program) [28] and refined by the full-matrix least-squares method on F^2 using SHELXL-2016 program [29] with the aid of the program WinGX 2021.3 [30]. H atoms bonded to C were generated stereochemically and refined by the riding model; those bonded to O and N were found in difference Fourier maps, and their coordinates were refined. To all H atoms, U_{iso} equal to 1.2 times U_{eq} of the carrier atom was given. The analysis of the crystal packing was performed using the program Mercury 2023.3.0 [31].

2.1.4. Hirshfeld Analysis

The Hirshfeld surface and potential energy surface were calculated using the program CrystalExplorer21.5 [32]. Crystallographic data for each X-ray single crystal were extracted from their crystallographic information files (.cif) and then imported into Crystal Explorer to produce the Hirshfeld surfaces. The settings used were as follows: property: none; resolution: high (standard). For fingerprint generation (di vs. de plot), we employed the following parameters: range-standard; filter-by elements; fingerprint-filter options are both inside–outside elements, including reciprocal contacts. Interactions in crystal structures with normalized contact distances shorter than the sum of the respective van der Waals radii of the atoms are depicted as red spots, while those with longer contacts exhibiting a positive d_{norm} value are represented in blue.

*2.2. Syntheses and Crystallization of Compounds **Triaz1-Triaz5***

Heterocycles such as triazoles and tetrazole are directly obtained from aminoguanidine [33]. Hereby, diaminoguanidine hydrochloride salt was used for the synthesis of 1,2,4-triazole compounds.

Triaz1: Commercial 2-pyrazinic acid (5.00 g, 40.3 mmol) and diaminoguanidine monohydrochloride (6.58 g, 52.4 mmol, 30% excess by mol) were finely ground in a mortar. The mixture was introduced incrementally with mechanical stirring into a beaker containing 40 g of polyphosphoric acid (PPA) at 100 °C. Whitin a short period, the reaction mixture began releasing gaseous HCl. The temperature of the resulting viscous mixture was raised to 150 °C, and the mixture underwent a 12 h reaction period while being continuously stirred. Subsequently, the mixture was transferred into 100 mL of cold water, and the pH of the resultant solution was adjusted to 5 by introducing a concentrated NaOH solution. The solid was isolated by vacuum filtration on paper filter, washed with cold water and dried in an oven at 100 °C overnight. A pale orange solid was obtained. Yield: 5.84 g (83%). M.p.: 277 °C. ^{1}H NMR (400 MHz, d6-DMSO) δ 5.94 (s, 2H), 6.04 (s, 2H), 7,50 (t, 1H), 8.91 (d, 1H). ^{13}C NMR (100 MHz, D6-DMSO) δ 143.2, 143.9, 144.0, 144.15, 145.2, 157.3. NMR spectra of **Triaz1** in Figures S1 and S2 (Supplementary Information).

Plate colorless crystals were obtained from the slow evaporation of an ethanolic solution at room temperature in 24 h.

Triaz2: Commercial 2-picolinic acid (5.00, 40.6 mmol) and diaminoguanidine monohydrochloride (7.36 g, 58.6 mmol, 30% excess by mol) were finely ground in a mortar. The mixture was introduced incrementally with mechanical stirring into a beaker containing 40 g of polyphosphoric acid (PPA) at 100 °C. Within a short period, the reaction mixture began releasing gaseous HCl. The temperature of the resulting viscous mixture was raised to 150 °C, and the mixture underwent a 12 h reaction period while being continuously stirred. Subsequently, the mixture was transferred into 100 mL of cold water, and the pH of the resultant solution was adjusted to 5 by introducing a concentrated NaOH solution. The solid was isolated by vacuum filtration on paper filter, washed with cold ethanol and dried in an oven at 100 °C overnight. A pale-yellow solid was obtained. Yield: 5.76 g (80.5%). M.p.: 239 °C. ^{1}H NMR (400 MHz, d6-DMSO) δ 5.85 (s, 2H), 6.11 (s, 2H), 6.93 (m, 4H), 7.25 (t, 3H), 7.86 (d, 2H), 8.36 (d, 2H), 11.88 (s, 1H). ^{13}C NMR (100 MHz, D6-DMSO) δ 114.7, 116.9, 118.5, 128.5, 129.9, 148.6, 155.6. NMR spectra of **Triaz2** in Figures S3 and S4 (Supplementary Information).

Plate colorless crystals were obtained from the slow evaporation of an ethanolic solution at room temperature in 24 h.

Triaz3-Triaz5: Diaminoguanidine monohydrochloride (5.00 g, 40 mmol, 15% excess by mol) was finely ground in a mortar and mixed with 1.65 mL of formic acid (94% m/V, 34.5 mmol). The mixture was heated at reflux for 2 h. The product was filtered under vacuum and washed with cold ethanol. A total of 2.730 g of **DATr-HCl** in the form of a white solid was obtained (80% Yield). M.p.: 250 °C. ^{1}H NMR (400 MHz, d6-DMSO) δ 6.26 (s, 2H), 8.32 (s, 2H), 8.42 (s, 1H). ^{13}C NMR (100 MHz, D6-DMSO) δ 142.2, 151.2. NMR spectra of **Triaz3** in Figures S5 and S6 (Supplementary Information).

A total of 40 mg (0.3 mmol) of **DATr-HCl** was dissolved in 10 mL of hot water, and 10 drops of HBr concentrated solution (48% v/v) were added. Prismatic colourless crystals of **Triaz3** were obtained by slow evaporation at room temperature in 2 days. The crystals were filtered off by vacuum filtration on paper filter, washed with cold ethanol and dried at room temperature under a fume hood overnight.

A total of 40 mg (0.3 mmol) of **DATr-HCl** was dissolved in 10 mL of hot water together with 34 mg (0.15 mmol) of $ZnBr_2$ (again, 2:1 molar ratio) and five drops of concentrated hydrobromic acid (48% v/v). Prismatic colourless crystals of **Triaz4** were obtained in a week by slow evaporation of the solvent at room temperature. The crystals were filtered off by vacuum filtration on paper filter, washed with cold ethanol and dried at RT under a fume hood overnight.

A total of 40 mg (0.3 mmol) of **DATr-HCl** was dissolved in 10 mL of hot water together with 21 mg (0.15 mmol) of $ZnCl_2$ (2:1 ratio by mol) and five drops of hydrochloric acid (37% v/v). The solution was left at room temperature for a week. The slow evaporation of the solvent led to the formation of prismatic colourless crystals of **Triaz5**. The crystals

were filtered off by vacuum filtration on paper filter, washed with cold ethanol and dried at room temperature under a fume hood overnight.

3. Results and Discussion

The crystal data of all studied triazoles are summarized in Table 1.

Table 1. Crystallographic information of the discussed compounds.

	Triaz1	**Triaz2**	**Triaz3**	**Triaz4**	**Triaz5**
Chemical Formula	$C_6H_7N_7$	$C_7H_9N_6 \cdot H_2O_4P$	$C_2H_6N_5 \cdot Br$	$2(C_2H_6N_5) \cdot Br_4Zn$	$2(C_2H_6N_5) \cdot Cl_4Zn$
M_r	177.19	274.19	180.03	585.25	407.41
Crystal system space group	Monoclinic, $P2_1/c$	Monoclinic, $C2/c$	Monoclinic, Cc	Monoclinic, Pc	Orthorhombic, $Pbca$
Temperature (K)	293	293	293	173	173
a, b, c (Å)	7.435(3), 9.067(3), 11.465(4)	26.400(7), 6.244(3), 18.701(6)	5.0140(17), 15.288(3), 7.937(2)	7.539(3), 12.059(4), 11.144(3)	16.9130(17), 8.348(4), 21.356(8)
α, β, γ (°)	90, 106.98(2), 90	90, 133.01(2), 90	90, 99.33, 90	90, 129.48(2), 90	90, 90, 90
V (Å^3)	739.2(5)	2254.3(15)	600.4(3)	782.0(5)	3015.2(18)
Z	4	8	4	2	8
Radiation type			Mo $K\alpha$		
μ (mm^{-1})	0.11	0.26	6.75	11.79	2.34
Crystal size (mm)	0.40 × 0.10 × 0.03	0.40 × 0.30 × 0.20	0.35 × 0.20 × 0.20	0.35 × 0.20 × 0.15	0.45 × 0.30 × 0.30
Diffractometer			Bruker-Nonius Kappa CCD		
Absorption correction			Multi-scan *SADABS*		
T_{min}, T_{max}	0.940, 0.980	0.890, 0.936	0.190, 0.327	0.112, 0.259	0.410, 0.528
$I > 2\sigma(I)$]	4695, 1677, 1203	10,432, 2582, 2015	1562, 1112, 1070	4720, 3082, 2918	11,619, 3392, 2787
R_{int}	0.042	0.038	0.022	0.050	0.031
sin $(\theta/\lambda)_{max}$ (Å^{-1})			0.650		
$R[F^2 > 2\sigma(F^2)]$, $wR(F^2)$, S	0.043, 0.110, 1.03	0.042, 0.102, 1.07	0.024, 0.061, 1.03	0.044, 0.119, 1.06	0.025, 0.054, 1.08
No. of reflections	1677	2582	1112	3082	3392
No. of parameters	130	184	92	168	202
No. of restraints	0	0	6	2	10
$\Delta\rho_{max}$, $\Delta\rho_{min}$ (e Å^{-3})	0.18, −0.24	0.27, −0.31	0.50, −0.49	1.27, −1.36	0.32, −0.38
Absolute structure			Flack x determined using 397 quotients [(I+) − (I−)]/[(I+) + (I−)]	Refined as an inversion twin.	
Absolute structure parameter			0.065(18)	0.05(3)	

The X-ray molecular structure of **Triaz1** is shown in Figure 1.

Both amino N atoms have a pyramidal geometry. In the case of CNH_2, the pyramidal geometry is more flat (sum of valence angles at N3 is 350(5)°) than for NNH_2 (sum of valence angles at N5 is 327(4)°). This is indicative of a partial π-conjugation of the CNH_2 amino group with the aromatic system of the triazole ring.

The molecular conformation of **Triaz1** is determined by the little twist around the C1-C5 bond, which produces a dihedral angle of 19.32(2)° between the average planes of the pyrazinyl and triazole moieties. The twist could account for the formation of suitable angles for the H-bond interactions of both N6 and N7 acceptor atoms. In fact, as shown in Figure 2a, the pyrazyl ring is involved in two strong hydrogen bond interactions between two layers of **Triaz1** with a distance of 2.438(3) and 2.269(2) Å. Diamminotriazole molecules in the layer are held by a strong homomeric $NCNH_2$ $R_2^2(8)$ motif [34–36], with a distance

of 2.305(2) Å. The 2_1 axis and the *c* glide plane build alternate layers of diaminotriazole molecules with a stacking distance of 3.288(5) (Figure 2b).

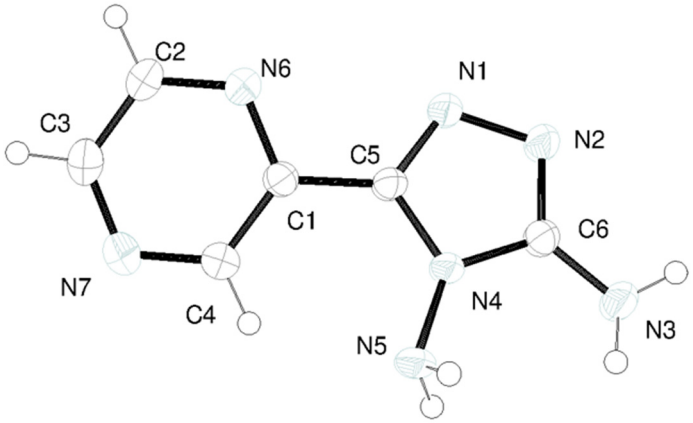

Figure 1. The X-ray molecular structure of **Triaz1** with displacement ellipsoids drawn at the 50% probability level.

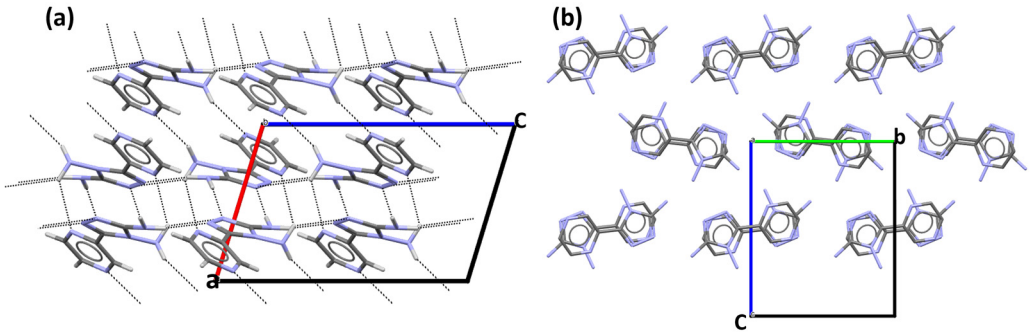

Figure 2. **Triaz1** crystal packing: (**a**) view along *b* axis; (**b**) view along *a* axis. Hydrogen bond interaction in dashed lines. Unit cell axis are drawn in stick lines (*a* axis in red, *b* axis in green, *c* axis in blue).

For a more in-depth examination of intermolecular interactions, we utilized the CrystalExplorer 21.5 program to calculate two-dimensional (2D) fingerprints and the corresponding Hirshfeld Surfaces (HS) for all the compounds. As depicted in Figure 3, the red areas on the HS signify close contacts in the shape of intermolecular hydrogen bonds, encompassing N···H and H···N interactions, which contribute to 46% of the crystal packing and confirm the significant role of homomeric synthons in the structure. The directional C···H close contacts are associated with the $\pi\cdots$H interaction of the aromatic rings with the surrounding molecules and contribute in all five compounds to less than 10%. The high value of H···H close contacts in this crystal structure could be associated with a close distance of the molecules in the crystal packing.

The X-ray molecular structure of **Triaz2** is shown in Figure 4.

Protonation of the triazole is at the N ring atom adjacent to the CNH_2 carbon, i.e., at N2. This feature, which holds unchanged for all singly protonated triazoles reported in this paper (*vide ultra*), is related to the stabilization of the positive charge on N2 by the electron donor NH_2 group on the adjacent carbon atom. As a result of this stabilization, the geometry around CNH_2 amino nitrogen is planar trigonal (the sum of valence angles at N3 is 358(7)°). On the other hand, the geometry around NNH_2 amino nitrogen is pyramidal, as in the neutral triazole (the sum of valence angles at N5 is 326(7)°).

The conformation of **Triaz2,** as for **Triaz1**, is characterized by a little twist of the pyridine ring with respect to the triazole ring, with the formation of a dihedral angle of 18.82(4)°. Differently from **Triaz1**, in this case the twist can be related to the ability of the triazole amino group close to the N6 to establish a strong H-bond interaction with the O_2

atom of the dihydrogen phosphate counter ion (Figure 5b). The cationic diaminotriazole molecules interact with the inorganic contour anion by establishing a strong heteromeric NH_2NCH POO $R_2^2(8)$ ring pattern, with distance values of 1.861(3), 2.014(3) and 2.171(3) Å (Figure 5a) [37–39]. Molecules in the crystal are arranged in a stair motif in which each diaminotriazole layer is linked to the other through the interaction with the counterion (Figure 5b). The tautomer that is isolated for this compound has a H atom bonded to N2 rather than N6, which is sterically hindered for this molecular conformation.

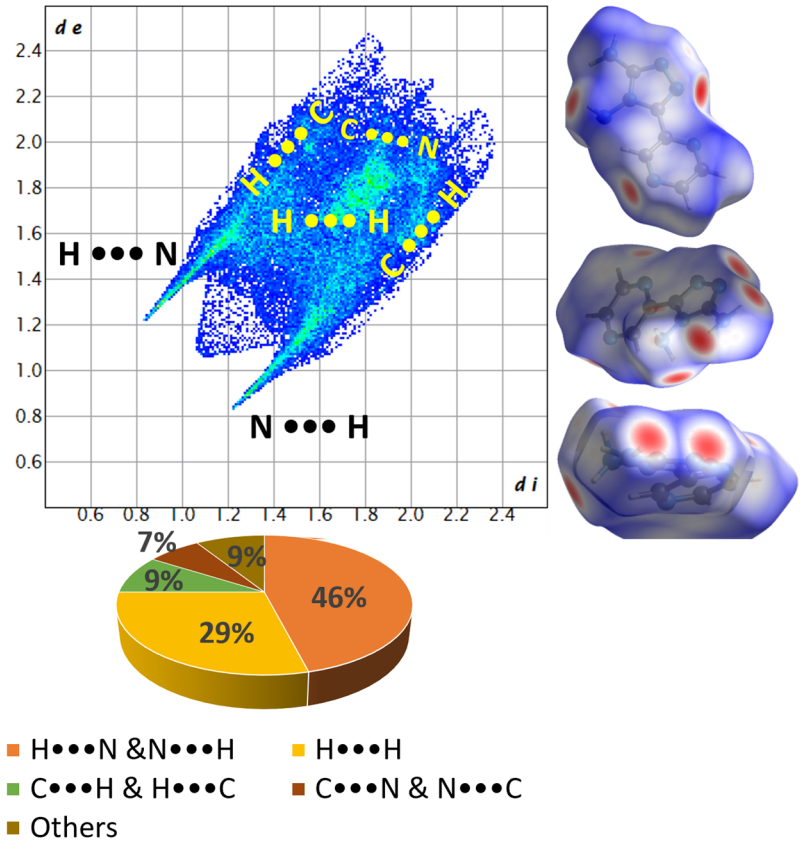

Figure 3. Hirshfeld fingerprint plot of the **Triaz1** compound with potential energy surface. d_i contact distances between nearest atoms present inside the surface; d_e contact distances between nearest atoms present outside the surface.

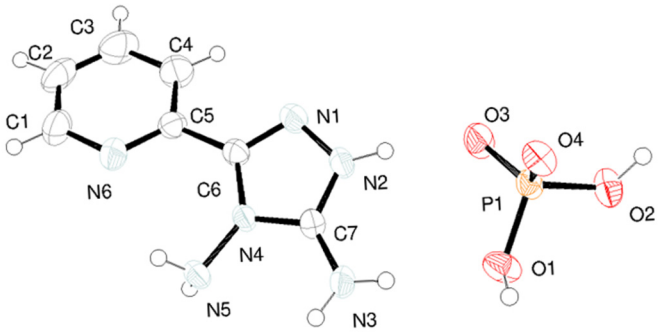

Figure 4. The crystal structure of **Triaz2** with displacement ellipsoids drawn at the 50% probability level.

The HS surface analysis, as shown in Figure 6, confirms that the packing is strongly influenced by the hydrogen bond interaction between the charged molecules, while differently from **Triaz1,** the N···H and H···N interactions are less relevant. For **Triaz2,** the highest value of H···H close contacts in the set of crystal structures studied in this paper is calculated.

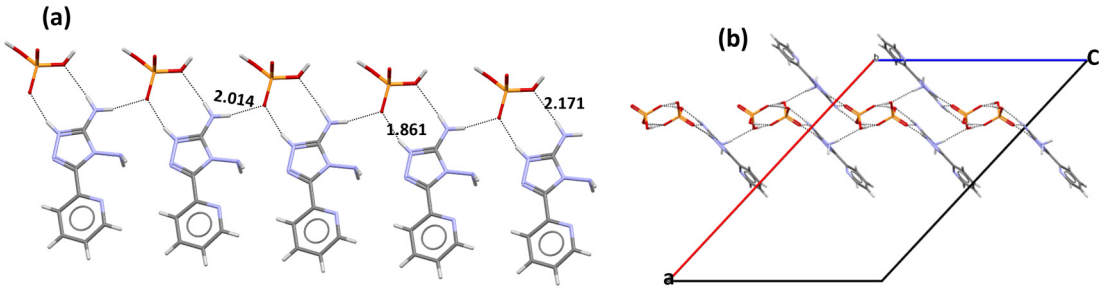

Figure 5. Triaz2 crystal packing: (**a**) Hydrogen bond interaction along the *b* axis; (**b**) view along the *b* axis. Hydrogen bond interaction in dashed lines. Unit cell axis are drawn in stick lines (*a* axis in red, *b* axis in green, *c* axis in blue).

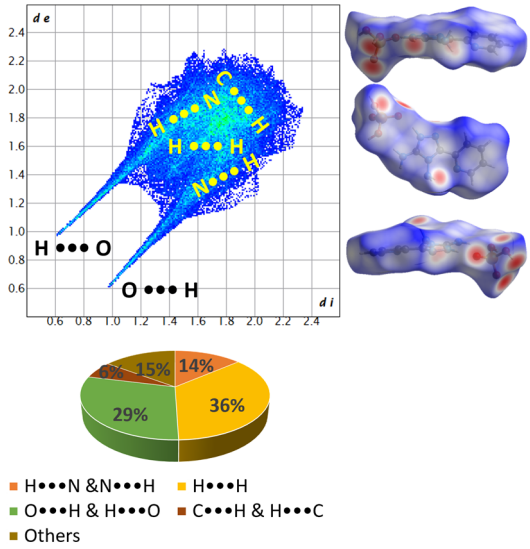

Figure 6. Hirshfeld fingerprint plot of **Triaz2** with potential energy surface. d_i contact distances between nearest atoms present inside the surface; d_e contact distances between nearest atoms present outside the surface.

Figure 7 shows the crystal structures of **Triaz3**, **Triaz4** and **Triaz5.**

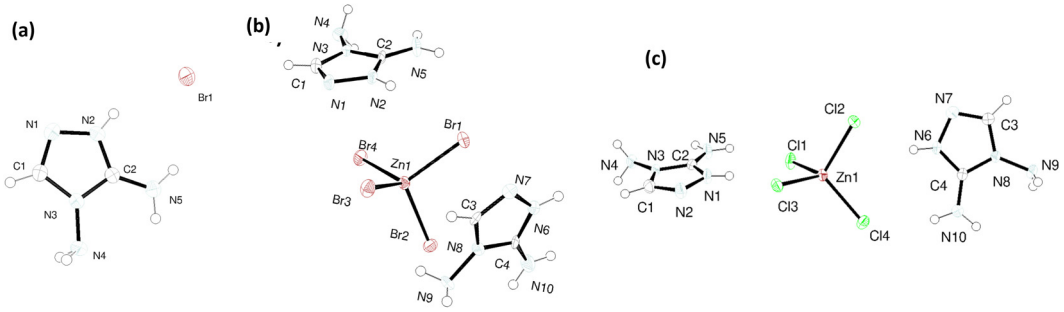

Figure 7. The crystal structures of (**a**) **Triaz3,** (**b**) **Triaz4** and (**c**) **Triaz5** with displacement ellipsoids drawn at the 50% probability level.

All three crystalline structures share the same diamminotriazole cation (**DATr**), but with three different counterions: bromide (Figure 7a), tretrachlobromide (Figure 7b) and tetrachlorozincate (Figure 7b), respectively. The counterions were chosen so as to obtain hybrid organic–inorganic molecular structures in which intermolecular interactions could favor crystalline packings with increasing densities, as these are desirable for High-Energy-Density materials. In fact, **Triaz3** and **Triaz4** have the highest crystallographic density

among the reported compounds, with values of **ρ** of 1.992 and 2.486 g/cm^3, respectively (ρ_{triaz1} = 1.592 g/cm^3, ρ_{triaz2} = 1.616 g/cm^3, ρ_{triaz5} = 1.795 g/cm^3). Therefore, the presence of bromide ion promotes a denser crystalline packing with a better angle and distance geometry. As previously stated, in all triazole cations, protonation is on the N ring atom adjacent to the CNH_2 carbon. As a result, the amino CNH_2 atom is planar trigonal (the sum of valence angles at N is always 360°), while NNH_2 keeps a pyramidal geometry, as in the neutral triazole **Triaz1** and protonated triazole of **Triaz2**.

The crystal packings are strongly influenced by hydrogen bond interactions between the **DATr** cation and the halogen of the counter ion (Figure 8), with the distances and angles reported in Table 2 confirmed by the HS fingerplot, which highlights a high contribution of these interactions with a maximum of 49% for **Triaz4** (Figure 9, center). On the other hand, **Triaz3** and **Triaz5** (Figure 9 left and right) show a major contribution of the N···H interaction, with 25% and 22%, respectively.

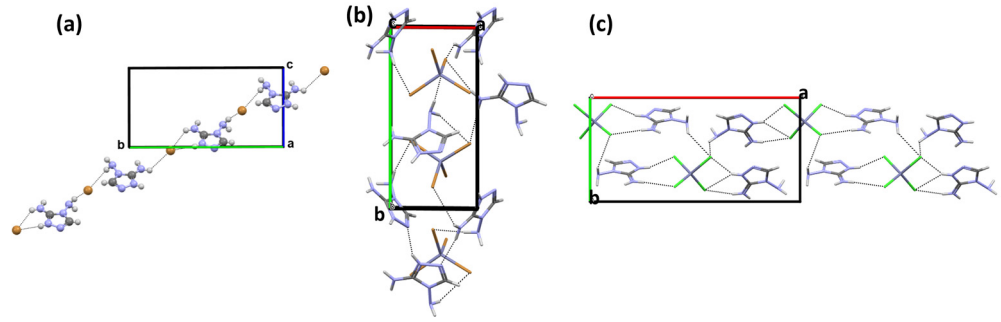

Figure 8. Hydrogen bonding patterns: (**a**) **Triaz3,** (**b**) **Triaz4** and (**c**) **Triaz5**. Hydrogen bond interactions in dashed lines. Unit cell axis are drawn in stick lines (*a* axis in red, *b* axis in green, *c* axis in blue).

Table 2. Hydrogen bond geometry of **Triaz3**, **Triaz4** and **Triaz5**.

	D—H···*A*	H···*A* (Å)	*D*—H···*A* (°)
Triaz3	N2—H2N···Br1	2.47(8)	155(7)
	N4—H4A···Br1	2.75(4)	147(6)
	N4—H4B···Br1	2.63(4)	157(5)
	N5—H5A···Br1	2.84(5)	138(6)
	N5—H5A···Br1	2.91(6)	123(6)
	N5—H5B···N1	2.12(4)	159(7)
Triaz4	C1—H1···Br1	2.65	166.6
	N2—H2···N4	2.18	165.5
	N4—H4A···Br2	2.65	166.0
	N4—H4B···Br1	2.44	162.8
	N5—H5A···Br4	2.68	145.9
	N5—H5B···N7	2.18	162.8
	N9—H9B···Br4	2.94	157.6
	N10—H10A···Br4	2.80	165.8
	N10—H10B···Br3	2.73	166.3
	N6—H6···N1	2.06	150.6
Triaz5	N1—H1N···Cl1	2.775(19)	132.5(2)
	N1—H1N···Cl3	2.584(18)	143.2(2)
	N4—H4A···Cl2	2.880(18)	142.8(2)
	N4—H4B···Cl3	2.782(19)	135.4(2)
	N5—H5A···Cl1	2.507(18)	149(2)
	N5—H5B···N7	2.113(16)	167(2)
	N6—H6N···Cl2	2.370(18)	150(2)
	N9—H9B···Cl3	2.654(18)	141.8(2)
	N10—H10A···Cl3	2.404(17)	176(2)
	N10—H10B···N2	2.63(3)	113(2)
	N10—H10B···Cl4	2.586(18)	158(2)

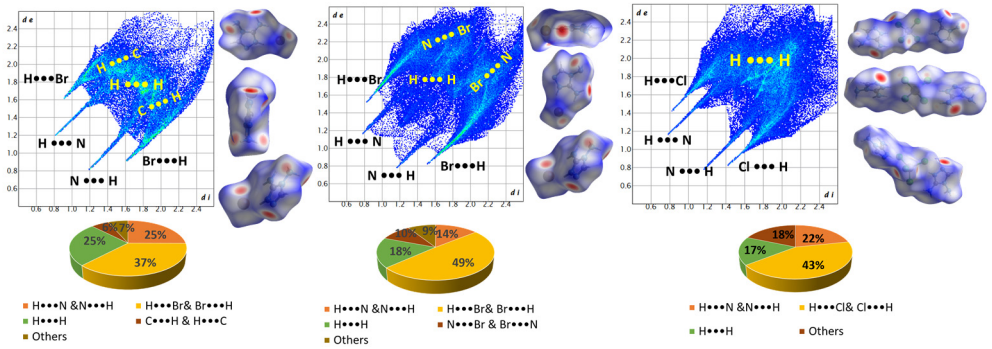

Figure 9. Hirshfeld fingerprint plot of **Triaz3** (**left**), **Triaz4** (**center**) and **Triaz5** (**right**) with potential energy surface. d_i contact distances between nearest atoms present inside the surface; d_e contact distances between nearest atoms present outside the surface.

The crystal packings of **Triaz3, Triaz4 and Triaz5** show a scaffold of inorganic counter anions spaced out by a scaffold of organic cations (Figure 10).

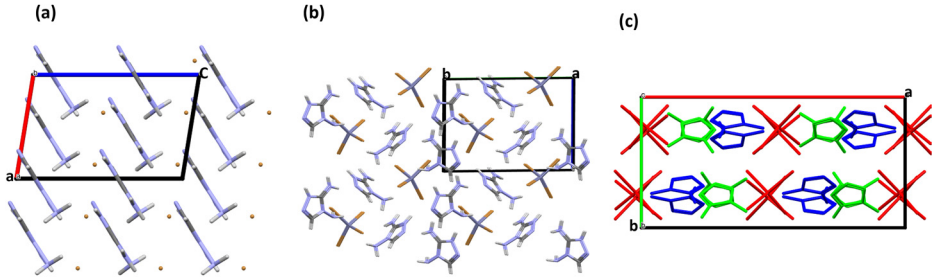

Figure 10. Crystal packing of (**a**) **Triaz3** along *b* axis, (**b**) **Triaz4** along *c* axis, and (**c**) **Triaz5** along *a* axis. Unit cell axis are drawn in stick lines (*a* axis in red, *b* axis in green, *c* axis in blue).

4. Conclusions

In conclusion, a novel series of N-Rich triazole derivatives, using the diaminoguanidine hydrochloride as a building block compound, were synthesized and crystallized. The purity of the synthetized compounds was determined by ^{1}H-NMR and ^{13}C-NMR spectroscopy. Altogether, five novel crystal structures were obtained and characterized by single X-ray diffraction measurements. The supramolecular features of the compounds were analyzed with a Hirshfeld topology that highlights a high presence of strong H-bonds driven by the amino group of the diaminotriazole moieties. **Triaz1** crystal packing is strongly driven by the homomeric $NCNH_2$ $R_2^2(8)$ supramolecular synthon, with a very high contribution (46%). Similarly, **Triaz2** crystal packing is influenced by the presence of the heteromeric NH_2NCH POO $R_2^2(8)$ ring pattern, with a contribution of 29%. The crystal packings of **Triaz3**, **Triaz4**, and **Triaz5** highlight the strong presence of strong H-bond interactions between the donor amino group of the triazole block and the halogen acceptor atoms of the counterions. These new systems, thanks to a high nitrogen content in the molecular backbone, could pave the way for a new series of materials that could be potentially relevant to industries involving high-energy-density materials, as an application in the field of explosives or propellant gases with low toxicity.

Supplementary Materials: The following supporting information can be downloaded at: https://www.mdpi.com/article/10.3390/cryst13121651/s1. ^{1}H NMR and ^{13}C NMR spectra of **Triaz1 (Figures S1 and S2)**, **Triaz2 (Figures S3 and S4)**, **DATr-HCl (Figures S5 and S6)** CCDC number of the deposited Crystal structure: 2304297, 2304298, 2304299, 2304303, 2304304.

Author Contributions: Conceptualization, E.P. and R.C.; methodology, E.P. and R.C.; software, E.P. and R.C.; validation, E.P. and R.C.; formal analysis, E.P. and R.C.; investigation, E.P. and R.C.; resources, R.C.; data curation, E.P. and R.C.; writing—original draft preparation, E.P.; writing—review and editing, R.C.;

visualization, E.P. and R.C.; supervision, R.C.; project administration, E.P. and R.C.; funding acquisition, R.C. All authors have read and agreed to the published version of the manuscript.

Funding: This research received no external funding.

Data Availability Statement: Data are contained within the article and supplementary materials.

Conflicts of Interest: The authors declare no conflict of interest.

References

1. Martins, P.; Jesus, J.; Santos, S.; Raposo, L.R.; Roma-Rodrigues, C.; Baptista, P.V.; Fernandes, A.R. Heterocyclic Anticancer Compounds: Recent Advances and the Paradigm Shift towards the Use of Nanomedicine's Tool Box. *Molecules* **2015**, *20*, 16852–16891. [CrossRef] [PubMed]
2. Heeger, A.J. Semiconducting Polymers: The Third Generation. *Chem. Soc. Rev.* **2010**, *39*, 2354–2371. [CrossRef] [PubMed]
3. Chen, J.; Kuang, J.; Liu, Y.; Yang, J.; Zhu, M.; Wei, X.; Shao, M.; Zhao, Z.; Guo, Y.; Liu, Y. Regioregular Pyridal[1,2,3]Triazole-Based Polymer Semiconductors for High Mobility and Near-Infrared Light Emission Applications. *Adv. Opt. Mater.* **2022**, *10*, 2201243. [CrossRef]
4. Miao, Q. Ten Years of N-Heteropentacenes as Semiconductors for Organic Thin-Film Transistors. *Adv. Mater.* **2014**, *26*, 5541–5549. [CrossRef] [PubMed]
5. Torres-Moya, I.; Arrechea-Marcos, I.; Tardío, C.; Carrillo, J.R.; Díaz-Ortiz, Á.; López Navarrete, J.T.; Ruiz Delgado, M.C.; Prieto, P.; Ortiz, R.P. D–A–D 2H-Benzo[d][1,2,3]Triazole Derivatives as p-Type Semiconductors in Organic Field-Effect Transistors. *RSC Adv.* **2018**, *8*, 21879–21888. [CrossRef] [PubMed]
6. Argeri, M.; Borbone, F.; Caruso, U.; Causà, M.; Fusco, S.; Panunzi, B.; Roviello, A.; Shikler, R.; Tuzi, A. Color Tuning and Noteworthy Photoluminescence Quantum Yields in Crystalline Mono-/Dinuclear ZnII Complexes. *Eur. J. Inorg. Chem.* **2014**, *2014*, 5916–5924. [CrossRef]
7. Fusco, S.; Parisi, E.; Volino, S.; Manfredi, C.; Centore, R. Redox and Emission Properties of Triazolo-Triazole Derivatives and Copper(II) Complexes. *J. Solut. Chem.* **2020**, *49*, 504–521. [CrossRef]
8. Nielsen, C.B.; Holliday, S.; Chen, H.Y.; Cryer, S.J.; McCulloch, I. Non-Fullerene Electron Acceptors for Use in Organic Solar Cells. *Acc. Chem. Res.* **2015**, *48*, 2803–2812. [CrossRef]
9. Kim, J.; Yun, A.J.; Gil, B.; Lee, Y.; Park, B. Triamine-Based Aromatic Cation as a Novel Stabilizer for Efficient Perovskite Solar Cells. *Adv. Funct. Mater.* **2019**, *29*, 1905190. [CrossRef]
10. Klapötke, T.M. *Chemistry of High-Energy Materials*, 5th ed.; Walter de Gruyter: Berlin, Germany, 2019.
11. Klapötke, T.M.; Schmid, P.C.; Schnell, S.; Stierstorfer, J. Thermal stabilization of energetic materials by the aromatic nitrogen-rich 4,4′,5,5′-tetraamino-3,3′-bi-1,2,4-triazolium cation. *J. Mater. Chem. A* **2015**, *3*, 2658–2668. [CrossRef]
12. Parisi, E.; Landi, A.; Fusco, S.; Manfredi, C.; Peluso, A.; Wahler, S.; Klapötke, T.M.; Centore, R. High-Energy-Density Materials: An Amphoteric N-Rich Bis(Triazole) and Salts of Its Cationic and Anionic Species. *Inorg. Chem.* **2021**, *60*, 21, 16213–16222. [CrossRef]
13. Hu, L.; Staples, R.J.; Shreeve, J.M. Energetic Compounds Based on a New Fused Triazolo[4,5-d]Pyridazine Ring: Nitroimino Lights up Energetic Performance. *Chem. Eng. J.* **2021**, *420*, 129839. [CrossRef]
14. Fusco, S.; Parisi, E.; Carella, A.; Capobianco, A.; Peluso, A.; Manfredi, C.; Borbone, F.; Centore, R. Solid State Selection between Nearly Isoenergetic Tautomeric Forms Driven by Right Hydrogen-Bonding Pairing. *Cryst. Growth Des.* **2018**, *18*, 6293–6301. [CrossRef]
15. Pagacz-Kostrzewa, M.; Bil, A.; Wierzejewska, M. UV-Induced Proton Transfer in 3-Amino-1,2,4-Triazole. *J. Photochem. Photobiol. A Chem.* **2017**, *335*, 124–129. [CrossRef]
16. Parisi, E.; Capasso, D.; Capobianco, A.; Peluso, A.; Di Gaetano, S.; Fusco, S.; Manfredi, C.; Mozzillo, R.; Pinto, G.; Centore, R. Tautomeric and Conformational Switching in a New Versatile N-Rich Heterocyclic Ligand. *Dalton Trans.* **2020**, *49*, 14452–14462. [CrossRef] [PubMed]
17. Parisi, E.; Centore, R. Stabilization of an Elusive Tautomer by Metal Coordination. *Acta Crystallogr. Sect. C* **2021**, *77*, 395–401. [CrossRef]
18. Capobianco, A.; Di Donato, M.; Caruso, T.; Centore, R.; Lapini, A.; Manfredi, C.; Velardo, A.; Volino, S.; Peluso, A. Phototautomerism of Triazolo-Triazole Scaffold. *J. Mol. Struct.* **2020**, *1203*, 127368. [CrossRef]
19. Sutradhar, M.; Alegria, E.C.B.A.; Mahmudov, K.T.; Guedes Da Silva, M.F.C.; Pombeiro, A.J.L. Iron(III) and Cobalt(III) Complexes with Both Tautomeric (Keto and Enol) Forms of Aroylhydrazone Ligands: Catalysts for the Microwave Assisted Oxidation of Alcohols. *RSC Adv.* **2016**, *6*, 8079–8088. [CrossRef]
20. Parisi, E.; Carella, A.; Borbone, F.; Chiarella, F.; Gentile, F.S.; Centore, R. Effect of Chalcogen Bonding on the Packing and Coordination Geometry in Hybrid Organic–Inorganic Cu(Ii) Networks. *CrystEngComm* **2022**, *24*, 2884–2890. [CrossRef]
21. Gentile, F.S.; Parisi, E.; Centore, R. Journeys in Crystal Energy Landscapes: Actual and Virtual Structures in Polymorphic 5-Nitrobenzo[c][1,2,5]Thiadiazole. *CrystEngComm* **2023**, *25*, 859–865. [CrossRef]
22. Centore, R.; Borbone, F.; Carella, A.; Causà, M.; Fusco, S.; Gentile, F.S.; Parisi, E. Hierarchy of Intermolecular Interactions and Selective Topochemical Reactivity in Different Polymorphs of Fused-Ring Heteroaromatics. *Cryst. Growth Des.* **2020**, *20*, 1229–1236. [CrossRef]

23. Fusco, S.; Capasso, D.; Centore, R.; Di Gaetano, S.; Parisi, E. A New Biologically Active Molecular Scaffold: Crystal Structure of 7-(3-Hydroxyphenyl)-4-Methyl-2H-[1,2,4]Triazolo[3,2-c][1,2,4]Triazole and Selective Antiproliferative Activity of Three Isomeric Triazolo-Triazoles. *Acta Crystallogr. C Struct. Chem.* **2019**, *75*, 1398–1404. [CrossRef]
24. Li, Z.M.; Zhang, J.G.; Cui, Y.; Zhang, T.L.; Shu, Y.J.; Sinditskii, V.P.; Serushkin, V.V.; Egorshin, V.Y. A Novel Nitrogen-Rich Cadmium Coordination Compound Based on 1,5-Diaminotetrazole: Synthesis, Structure Investigation, and Thermal Properties. *J. Chem. Eng. Data* **2010**, *55*, 3109–3116. [CrossRef]
25. Emilsson, K.; Selander, L.H. Bho. *Eur. J. Med. Chem.* **1986**, *21*, 235.
26. Trust, R.I.; Albright, J.D.; Lovell, F.M.; Perkinson, N.A. 6- and 7-Aryl-1,2,4-Triazolo[4,3-b]-1,2,4-Triazines. Synthesis and Characterization. *J. Heterocycl. Chem.* **1979**, *16*, 1393–1403. [CrossRef]
27. Bruker-Nonius. *SADABS*; Bruker-Nonius: Delft, The Netherlands, 2002.
28. Altomare, A.; Burla, M.C.; Camalli, M.; Cascarano, G.L.; Giacovazzo, C.; Guagliardi, A.; Moliterni, A.G.G.; Polidori, G.; Spagna, R. SIR97: A New Tool for Crystal Structure Determination and Refinement. *J. Appl. Crystallogr.* **1999**, *32*, 115–119. [CrossRef]
29. Sheldrick, G.M. Crystal Structure Refinement with SHELXL. *Acta Crystallogr. C Struct. Chem.* **2015**, *71*, 3–8. [CrossRef]
30. Farrugia, L.J. WinGX and ORTEP for Windows: An Update. *J. Appl. Crystallogr.* **2012**, *45*, 849–854. [CrossRef]
31. Macrae, C.F.; Bruno, I.J.; Chisholm, J.A.; Edgington, P.R.; McCabe, P.; Pidcock, E.; Rodriguez-Monge, L.; Taylor, R.; Van De Streek, J.; Wood, P.A. Mercury CSD 2.0—New Features for the Visualization and Investigation of Crystal Structures. *J. Appl. Crystallogr.* **2008**, *41*, 466–470. [CrossRef]
32. Spackman, M.A.; Jayatilaka, D. Hirshfeld Surface Analysis. *CrystEngComm* **2009**, *11*, 19–32. [CrossRef]
33. Lieber, E.; Smith, G.B.L. The Chemistry of Aminoguanidine and Related Substances. *Chem. Rev.* **2002**, *25*, 213–271. [CrossRef]
34. Kennedy, A.R.; Khalaf, A.I.; Suckling, C.J.; Waigh, R.D. Methyl 2-Amino-5-Isopropyl-1,3-Thiazole-4-Carboxylate. *Acta Crystallogr. Sect. E* **2004**, *60*, o1510–o1512. [CrossRef]
35. Stierstorfer, J.; Tarantik, K.R.; Klapötke, T.M. New Energetic Materials: Functionalized 1-Ethyl-5-Aminotetrazoles and 1-Ethyl-5-Nitriminotetrazoles. *Chem.—A Eur. J.* **2009**, *15*, 5775–5792. [CrossRef] [PubMed]
36. Wang, C.; Hu, S.; Sun, C.C. Expedited Development of a High Dose Orally Disintegrating Metformin Tablet Enabled by Sweet Salt Formation with Acesulfame. *Int. J. Pharm.* **2017**, *532*, 435–443. [CrossRef]
37. Kaynak, F.B.; Eriksson, L.; Salgın-Gökşen, U.; Gökhan-Kelekçi, N. Molecular Structure of 2-Methylamino-5-[(5-Methyl-2-Benzoxazolinone-3-Yl)Methyl]-1,3,4-Thiadiazole Dihydrophosphate: A Combined X-ray Crystallographic and Ab Initio Study. *Struct. Chem.* **2008**, *19*, 757–764. [CrossRef]
38. Matulková, I.; Fábry, J.; Eigner, V.; Dušek, M.; Kroupa, J.; Němec, I. Isostructural Crystals of Bis(Guanidinium) Trioxofluoro-Phosphate/Phosphite in the Ratio 1/0, 0.716/0.284, 0.501/0.499, 0.268/0.732, 0/1—Crystal Structures, Vibrational Spectra and Second Harmonic Generation. *Crystals* **2022**, *12*, 1694. [CrossRef]
39. Radanović, M.M.; Rodić, M.V.; Armaković, S.; Armaković, S.J.; Vojinović-Ješić, L.S.; Leovac, V.M. Pyridoxylidene Aminoguanidine and Its Copper(II) Complexes—Syntheses, Structure, and DFT Calculations. *J. Coord. Chem.* **2017**, *70*, 2870–2887. [CrossRef]